


## Strong noise limit for population dynamics in incompressible advection

Giorgia Guccione<sup>1,2</sup>, Roberto Benzi<sup>2</sup>, and Federico Toschi<sup>1,3</sup>

<sup>1</sup>*Department of Applied Physics, Eindhoven University of Technology, 5600 MB Eindhoven, Netherlands*

<sup>2</sup>*Department of Physics and INFN, University of Tor Vergata, 00133 Rome, Italy*

<sup>3</sup>*CNR-IAC, 00185 Rome, Italy*

 (Received 17 October 2020; revised 3 July 2021; accepted 31 August 2021; published 30 September 2021)

Genetic diversity is at the basis of the evolution process of populations and it is responsible for the populations' degree of fitness to a particular ecosystem. In marine environments many factors play a role in determining the dynamics of a population, including the amount of nutrients, the temperature, and many other stressing factors. An important and yet rather unexplored challenge is to figure out the role of individuals' dispersion, due to flow advection, on population genetics. In this paper we focus on two populations, one of which has a slight selective advantage, advanced by an incompressible two-dimensional flow. In particular, we want to understand how this advective flow can modify the dynamics of the advantageous allele. We generalize, through a theoretical analysis, previous evidence according to which the fixation probability is independent of diffusivity, showing that this is also independent of fluid advection. These findings may have important implications in the understanding of the dynamics of a population of microorganism, such as plankton or bacteria, in marine environments under the influence of (turbulent) currents.

DOI: [10.1103/PhysRevE.104.034421](https://doi.org/10.1103/PhysRevE.104.034421)

### I. INTRODUCTION

Quantitative descriptions of evolutionary dynamics and population genetics are fundamental issues in understanding genetic diversity in the real world. Focusing on the simplest case of two competing populations, the pioneering works of Kimura *et al.* [1–3] provide a clear-cut answer in the well-mixed (zero-dimensional) case.

To establish the notation and explain in some detail both the model and the problem we discuss in this paper, we consider two populations, say,  $A$  and  $B$ , which can reproduce and die according to one of the many possible models. Here we choose the framework reviewed by Korolev *et al.* [4]. Ignoring spatial effects, let us denote by  $N_A$  and  $N_B$  the numbers of individuals in the system. In the neutral case, we consider both species with the same dynamics, i.e., individuals reproduce at a rate  $\mu$  and die at a rate  $\mu(N_A + N_B)$ . Notice that, in general, the value of  $\mu$  may be different for the rates of reproduction and death. Here we choose the same rate to simplify the notation and the algebra (see [5] for a more general description). We also assume that both individuals cannot grow more than some limiting value. We can introduce a selective advantage for one of the two species, say,  $A$ , in several ways. Following [4,5], we assume that the selective advantage  $s$  is induced by a faster birth rate  $\mu(1 + s)$  for the individual  $A$ . Since the model is defined in terms of the rates of reproduction and death, the basic mathematical formulation should be defined in terms of a master equation for the different transition probabilities from one state  $N_A$  or  $N_B$  to a different one. Then using the Kramers-Moyal expansion, we can obtain a Fokker-Planck equation for the probability  $P(N_A, N_B, t)$  to observe a number of  $N_A$  and  $N_B$  individuals at time  $t$  (a detailed derivation is provided in Appendix A of [5]). From the Fokker-Planck equation, we can obtain the associated stochastic differential

equations. Finally, upon introducing the population fraction  $f = N_A/(N_A + N_B)$  and assuming  $s$  to be small, we can derive the stochastic differential equation

$$\partial_t f = \mu s f(1 - f) + \left[ \frac{2\mu}{N} f(1 - f) \right]^{1/2} \eta(t), \quad (1)$$

where  $N$  is the whole population size and  $\eta(t)$  is a Gaussian random variable,  $\delta$  correlated in time with zero mean and unit variance. Equation (1) is a stochastic differential equation with multiplicative noise, to be interpreted with the Itô prescription, and there exist two absorbing boundaries  $f = 1$  and  $f = 0$ . We remark that, since the noise variance is proportional to  $\mu$ , the timescale  $1/\mu$  becomes irrelevant, i.e., the statistical properties of (1) depend on time through the dimensionless combination  $t\mu$ . Assuming that at time  $t = 0$  the initial population fraction is  $f_0$ , we are interested in computing the fixation probability  $P_{\text{fix}}$  for the species  $A$  with selective advantage  $s$  to overcome the whole population size (fixation) and average time  $T_{\text{fix}}$  for the fixation to occur. This computation can be exactly done by solving the backward Kolmogorov equation of the stochastic differential equation, as it was shown for the first time by Kimura *et al.* [1]. Upon denoting by  $f_0$  the initial relative fraction of a population with a small selective advantage  $s$ , the fixation probability  $P_{\text{fix}}$  for advantageous population and the average time  $T_{\text{fix}}$  to reach fixation, for small  $s$ , are given by

$$P_{\text{fix}} = \frac{1 - \exp(-f_0 s N)}{1 - \exp(-s N)}, \quad (2)$$

$$T_{\text{fix}} = \frac{N f_0}{\mu(1 - f_0)} \ln \left( \frac{1}{f_0} \right). \quad (3)$$

More complex and therefore interesting features arise if one considers the effect of spatial structure. Following Korolet *et al.* [4], we consider a system in a bounded domain  $L^d$  of dimension  $d = 1, 2$ . Next we divide the system into small boxes (demes) of size  $a^d$ . In each deme, the maximum population size is denoted by  $N_0$ . Diffusion effects can be easily introduced by assuming a rate of migration from one deme to the nearest neighborhood. The continuous limit is achieved for  $L/a \gg 1$ . Then Eq. (1) is formulated in terms of  $f(\vec{x}, t)$ , which is the local relative fraction of  $A$  with respect to the local population size. Using the same approach shortly reviewed above, we can derive the celebrated Fisher-Kolmogorov-Petrovsky-Piscounov (FKPP) equation

$$\partial_t f = D\Delta f + \mu s f(1 - f) + \left[ \frac{2\mu f(1 - f)}{N_0} \right]^{1/2} w(\vec{x}, t), \quad (4)$$

where  $w(\vec{x}, t)$  is a white noise  $\delta$  correlated in space and time and  $D$  is the diffusion [see [5] for a detailed derivation of Eq. (4)].

A rather nontrivial result was obtained by Doering *et al.* [6], who showed that the probability of fixation  $P_{\text{fix}}$  for the stochastic FKPP equation in  $d = 1$  does not depend on the diffusivity (in the limit of small  $D$  and large total population size). The same outcome seems to hold for the two-dimensional case  $d = 2$ , according to the investigations presented by [5,7]. For the one-dimensional problem, in the strong noise limit that is characterized by small values of  $D$  and population density  $N_R$ , it has been proved that an initially localized population  $f(\vec{x}, t)$  propagates in space with a velocity  $v_s \sim DN_R s/a \ll v_F \equiv \sqrt{Ds/\mu}$ , where  $v_F$  is the Fisher velocity [6,8]. We want to show that the slowdown of front propagation and the segregation effects induced by the fluctuations due to the noise (see [4]) are able to explain why  $P_{\text{fix}}$  is independent of  $D$ .

Much less is known when a population is subject to the advection of an incompressible velocity field  $\vec{v}$ , when the total concentration  $c$  is uniform over the domain ( $c = 1$ ). In this case, the describing equation becomes

$$\partial_t f + \vec{v} \cdot \vec{\nabla} f = D\Delta f + \mu s f(1 - f) + \left[ \frac{2\mu f(1 - f)}{N_0} \right]^{1/2} w(\vec{x}, t), \quad (5)$$

where  $\vec{v}$  is assumed to be a two-dimensional incompressible flow, with  $\text{div}(\vec{v}) = 0$ . In this paper we are interested in discussing whether the advection of an incompressible two-dimensional flow can modify the Darwinian dynamics of an advantageous allele and in particular we study how  $P_{\text{fix}}$  and  $T_{\text{fix}}$  may change. For our purpose, we consider  $f(\vec{x}, 0) \equiv f_0$  uniform in space and we assume periodic boundary conditions in a two-dimensional domain of size  $L^2$ . Because advection, stationary or not, can always increase the effective dispersion (diffusivity) of individuals, we do not expect  $P_{\text{fix}}$  to change with respect to the results previously discussed. The situation may be different for the fixation timescale of the system, i.e.,  $T_{\text{fix}}$ .

In this section we summarize some of the key findings obtained in the paper. In the case without advection, the strong noise limit is shown to occur when the following inequality

holds:

$$\frac{a^2}{N_0 D} \gg \frac{1}{\mu}. \quad (6)$$

The physical interpretation of Eq. (6) is rather clear:  $t_D \equiv a^2/D$  is the diffusive characteristic time needed for a particle to spread, on average, over a distance of order  $a$ ,  $1/\mu$  is the generation time, and  $N_0/\mu$  is proportional to the inverse of the noise variance in Eq. (4). When the multiplicative noise is large (small  $N_0$  or large  $\mu$ ), the effect of the noise (due to the random processes of death and birth in the population) is large and the diffusion becomes relevant on a timescale corresponding to several generation times in the population dynamics. Then competition in space occurs at a much slower rate when the inequality (6) is satisfied and, as shown in Sec. II, the relevant timescale in the system becomes  $N_0 D/a^2$ . It follows that the fixation time  $T_{\text{fix}}$  is given by

$$T_{\text{fix}} = \frac{L^2}{D} \frac{f_0}{1 - f_0} \ln \left( \frac{1}{f_0} \right), \quad (7)$$

which can be compared to Eq. (3), with  $L^2/D$  replacing  $N/\mu$ .

When advection is present, the proper analysis can be done by considering the effective (or eddy) diffusivity  $D_{\text{eff}}$  due to the flow and its related characteristic spatial scale  $l_u$ . Knowing the advection field, it is difficult to compute exactly  $D_{\text{eff}}$  and  $l_u$ . In a few cases, as we discuss in this paper, it is possible to obtain an analytical estimate for both quantities (see [9] for details). In this study we will provide theoretical and numerical evidence that there may exist a strong noise scenario for the dynamics if the following inequality is fulfilled:

$$\frac{l_u^2}{D_{\text{eff}} N_0} \gg \frac{1}{\mu}. \quad (8)$$

The physical motivation behind Eq. (8) can be obtained by considering the case  $s = 0$  in Eq. (5). Then the effect of a nonuniform advection introduces a characteristic timescale  $t_u$  for the effective diffusion of a particle in the system. Equation (8) states that if  $t_u \equiv l_u^2/D_{\text{eff}}$  is much longer than the generation timescale  $1/\mu$  and  $N_0$  is relatively small, the effect of advection occurs on a timescale corresponding to several generation times in the population dynamics. As already noticed,  $N_0/\mu$  is proportional to the inverse of the variance due to multiplicative noise in Eq. (5). Then we can physically argue that (8) is equivalent to the strong noise condition in the system, similarly to our previous analysis of Eq. (6). Note that we expect the relation  $a^2/D = t_D > t_u = l_u^2/D_{\text{eff}}$ . The physical interpretation of (8) suggests, by analogy, that, in the presence of advection, a proper estimate for the fixation time  $T_{\text{fix},v}$ , for small  $s$ , is given by

$$T_{\text{fix},v} = \frac{N_T l_u^2}{D_{\text{eff}} N_0} \frac{f_0}{1 - f_0} \ln \left( \frac{1}{f_0} \right). \quad (9)$$

Because  $t_D > t_u$ , we expect  $T_{\text{fix},v}$  to be shorter than the  $T_{\text{fix}}$  given by (7) but still much longer than the fixation time for the well-mixed population given by Eq. (3).

In general, the theoretical computation of  $D_{\text{eff}}$  is not a simple task (see [9]). For the relatively simple case of chaotic flows one usually finds that  $D_{\text{eff}} \sim u_0 l_u$ , with  $u_0$  being some

typical velocity. Then Eq. (8) can be written as

$$\text{Da} \equiv \frac{\mu l_u}{u_0} \gg N_0, \quad (10)$$

where  $\text{Da}$  is the so-called Damköhler number representing the ratio between the rate of growing with respect to the characteristic rate of population spreading (see also [10,11] for studies of thin front propagation in steady and unsteady cellular flow and no genetic fluctuations, i.e.,  $N_0 \rightarrow \infty$ ). For finite  $\text{Da} \gg N_0$  strong noise effects characterize the dynamics in the presence of chaotic advection.

Using  $D_{\text{eff}} \sim u_0 l_u$ , one can think of  $l_u/u_0$  as the so-called eddy turnover time at scale  $l_u$  of the flow. If the flow is characterized by a single spatial scale  $l_u$ , Eq. (10) becomes a condition on the velocity scale  $u_0$ . However, for turbulent flows, the eddy turnover time increases with  $l$ : Whereas at small  $l$  the system behaves as in the well-mixed case (turbulence increases mixing and no strong noise effects can arise), there may exist some critical scale above which strong noise effects become relevant. We will discuss this interesting possibility in some detail in Sec. V, although a systematic and quantitative investigation of this point is definitively outside the aim of this paper.

In the next section we present a theoretical framework to support our findings, i.e., Eqs. (6) and (8)–(10). This framework is validated by numerical simulations in Sec. III. In Sec. IV we summarize our results and we discuss their relevance in the case of population dynamics of oceanic phytoplankton subjected to marine turbulence. All the numerical simulations are based on the method discussed by [12]. As already noted,  $1/\mu$  is the only timescale for the population dynamics and we can set  $\mu = 1$  without loss of generality.

## II. THEORY

We consider two populations  $A$  and  $B$  in a two-dimensional closed system of size  $L \times L$  endowed with periodic boundary conditions. Let  $C_A$  and  $C_B$ , with  $C_A + C_B = 1$ , denote the relative time- and space-dependent concentrations. The two populations are advected by an incompressible velocity field. The dynamics of a population is well described by the continuum stochastic Fisher equation in terms of diffusion  $D$ , logistic growth  $\mu$ , selective advantage  $s$ , and advection  $\vec{v}$ . Upon denoting by  $f$  the fraction of the concentration of a species over the total concentration,  $f \equiv C_A/(C_A + C_B)$ , the discretized form of the equation governing the dynamics of the two populations reads

$$\frac{\partial f}{\partial t} + \vec{v} \cdot \vec{\nabla} f = D \Delta f + \mu s f(1-f) + \left[ \frac{2\mu}{N_0} f(1-f) \right]^{1/2} w(\vec{x}, t), \quad (11)$$

where  $N_0$  is the total number of organisms per deme and  $w(\vec{x}, t)$  is a Gaussian random process  $\delta$  correlated both in space and in time. Given the deme size  $a$ , Eq. (11) can be discretized on a regular grid of  $n$  points, where  $n = L/a$ , with  $L$  the domain size (see Appendix A for an extensive explanation). For a two-dimensional case, there exist  $N = n \times n$  demes in the domain. In the following we will use the notation

$f_i$ , with  $i = 1, 2, \dots, N$ , to indicate the value of  $f(x, y, t)$  in the deme  $i$  and consequently  $\vec{\nabla} f_i$ ,  $\Delta f_i$  denoting values of  $\vec{\nabla} f$  and  $\Delta f$  in the same deme. The divergence of the velocity field is assumed to be zero. Then, upon averaging Eq. (11) in space and denoting by  $f(m)$  the space average of  $f(x, y, t)$ , we obtain

$$\frac{\partial f(m)}{\partial t} = \mu s \langle H \rangle + \left[ \frac{2\mu}{N_T} \langle H \rangle \right]^{1/2} w(t), \quad (12)$$

where  $N_T = N_0 N$ ,  $w(t)$  is a Gaussian random process  $\delta$  correlated in time, and

$$H \equiv f(x, y, t)[1 - f(x, y, t)], \quad (13)$$

$$\langle \dots \rangle \equiv \frac{1}{L^2} \int \dots dx dy. \quad (14)$$

In order to obtain the noise variance on the right-hand side of Eq. (12), we define the noise term acting on  $f(m)$  as

$$\frac{1}{N} \sum_i \left[ \frac{2\mu}{N_0} f_i(1-f_i) \right]^{1/2} w_i \equiv \frac{1}{N} \sum_i \sigma_i w_i, \quad (15)$$

where  $\sigma_i$  is equivalent to  $[\frac{2\mu}{N_0} f_i(1-f_i)]^{1/2}$  and  $w_i$  is shorthand for the noise acting on deme  $i$ . Since  $\langle w_i w_j \rangle = \delta_{ij}$ , the variance of the noise term (15) is given by

$$\left\langle \frac{1}{N^2} \sum_{i,j} \sigma_i \sigma_j w_i w_j \right\rangle = \frac{2\mu}{N_0 N^2} \sum_i f_i(1-f_i) = \frac{2\mu}{N_0 N} \langle H \rangle. \quad (16)$$

The space averaged  $\langle H \rangle$  can also be written as

$$\langle H \rangle = H(f(m)) - \langle (\delta f)^2 \rangle, \quad (17)$$

where  $H(f(m)) = f(m)[1 - f(m)]$  and  $\delta f \equiv f(x, y, t) - f(m)$ . Following the results discussed in Refs. [8,13], for small values of the selective advantage  $s$ , we can obtain useful insight into the dynamics of the system by considering the equation for  $H$  at  $s = 0$ , namely,

$$\frac{\partial H}{\partial t} + \vec{v} \cdot \vec{\nabla} H = D \Delta f - 2Df \Delta f - \frac{2\mu}{N_0} f(1-f) + \dots, \quad (18)$$

where the third term on the right-hand side of Eq. (18) is derived from the application of Itô's calculus and the ellipsis represents all the terms due to noise. Next we perform a space averaging. Because of the periodic boundary conditions and the incompressibility of the advection field, we can use the identities  $\langle \Delta f \rangle = 0$ ,  $\langle \vec{v} \cdot \vec{\nabla} H \rangle = \langle \text{div}(\vec{v}H) \rangle = 0$ , and  $-\langle f \Delta f \rangle = \langle (\vec{\nabla} f)^2 \rangle$ . The final result is achieved by (i) averaging Eq. (18) over the noise realizations, which allows us to neglect the noise, and (ii) neglecting the time derivative  $\partial_t \langle H \rangle$ , which rapidly goes to zero both in one and in two dimensions (see [4] for details).

Then the final result reads

$$D \langle (\vec{\nabla} f)^2 \rangle = \frac{\mu}{N_0} \langle H \rangle. \quad (19)$$

This equation, for  $\vec{v} = 0$ , has been also derived in Refs. [4,14]. Let us also remark that Eq. (19) is formally independent of

$\vec{v}$ . The effect of velocity advection (if any) shows up in the following steps.

Now we introduce the timescale  $t_*$ , which is defined by the relation

$$D\langle(\vec{\nabla}f)^2\rangle \equiv \frac{1}{t_*}\langle(\delta f)^2\rangle. \quad (20)$$

Using Eq. (20) in Eq. (17), we can compute  $\langle H \rangle$  as a function of  $H(f(m))$  and we obtain

$$\langle H \rangle = H(f(m)) - \frac{\mu t_*}{N_0}\langle H \rangle. \quad (21)$$

Solving Eq. (21) for  $\langle H \rangle$ , it turns out that

$$\langle H \rangle = AH(f(m)), \quad (22)$$

where

$$A = \frac{1}{1 + \frac{\mu t_*}{N_0}}. \quad (23)$$

Using Eq. (22), we now can express  $\langle H \rangle$  as  $H(f(m) = f(m)[1 - f(m)])$ . We insert it in Eq. (12), obtaining

$$\frac{\partial f(m)}{\partial t} = sA\mu f(m)[1 - f(m)] + \left[ \frac{2\mu A}{N_T} H(f(m)) \right]^{1/2}. \quad (24)$$

The key quantity to consider in the following is the ratio  $G \equiv \mu t_*/N_0$ . For  $G \ll 1$  and Eq. (23), we obtain  $A \sim 1$ . Equation (24) reduces to the case of a well-mixed population with selective advantage  $s$ . In contrast, for  $G \gg 1$  we get  $A\mu \sim N_0/t_*$  and the characteristic time of the system dynamics depends explicitly on both  $N_0$  and  $t_*$ ; this is the case referred to as the strong noise limit where the genetic drift (i.e., space-dependent number fluctuations in the population size) becomes important.

To make progress, we start analyzing the case  $\vec{v} = 0$ , i.e., the case where  $t_* = t_D$ . In this case, the effect of random perturbations, caused by the growth and death processes of a population, within each single deme, implies that the concentration gradients must be of order  $1/a$ .

A reasonable guess on  $t_D$  may be derived by considering, as a guideline, the two-dimensional stochastic differential equation

$$\partial_t \phi = D\Delta\phi + \sqrt{\epsilon}w(\vec{x}, t). \quad (25)$$

Assuming that there exists an ‘‘ultraviolet’’ cutoff  $k_M$ , it is possible to exactly compute the ratio  $\langle(\vec{\nabla}\phi)^2\rangle/\langle(\phi)^2\rangle$ , obtaining

$$\frac{\langle(\vec{\nabla}\phi)^2\rangle}{\langle(\phi)^2\rangle} \sim k_M^2. \quad (26)$$

(Mathematical details for the  $k_M$  introduction will be treated in Appendix B.) From the above insight, using  $k_M \sim 1/a$ , we have

$$t_*(\vec{v} = 0) \equiv t_D \sim \frac{a^2}{D}. \quad (27)$$

Through the use of Eqs. (27), (23), and (24) we are led to the result

$$\frac{\partial f(m)}{\partial t} = \frac{\mu}{1 + \frac{\mu}{N_R D}} s f(m)[1 - f(m)] + \left[ \frac{2}{N_T} \frac{\mu}{1 + \frac{\mu}{N_R D}} f(m)[1 - f(m)] \right]^{1/2}, \quad (28)$$

where  $N_R = N_0/a^2 \equiv N_T/L^2$  is the population density.

The strong noise limit for Eq. (28) is expressed by the condition  $\mu a^2/N_0 D = \mu/N_R D \gg 1$ , which corresponds to Eq. (6). In the strong noise limit, Eq. (28) becomes

$$\frac{\partial f(m)}{\partial t} = N_R D s f(m)[1 - f(m)] + \left[ \frac{2N_R D}{N_T} f(m)[1 - f(m)] \right]^{1/2}. \quad (29)$$

Using Eq. (28) or (29), we can immediately deduce that the fixation probability  $P_{\text{fix}}$  can be derived from the Kimura theory [1] for well-mixed population, through Eq. (2) to derive  $P_{\text{fix}}$  in our space-dependent dynamics. Remarkably, a simple computation shows that  $P_{\text{fix}}$  is independent of the diffusivity  $D$ . This is a rather remarkable result, first predicted by Doering *et al.* [13] for the one-dimensional problem in the strong noise limit and observed in Refs. [7,15] in both one and two dimensions. Here we get a clear-cut explanation for this result.

Due to Eq. (28) or (29), we derive that for both cases, strong and weak noise, the probability of fixation  $P_{\text{fix}}$  can be computed from knowing  $N_T$  and the space average of the initial population fraction, hereafter denoted by  $f(m, 0)$ . Using (2) we get

$$P_{\text{fix}} = \frac{1 - e^{-sN_T f(m,0)}}{1 - e^{-sN_T}}. \quad (30)$$

Next we can rewrite  $N_T f(m, 0) = N_R \int dx dy f(x, y, 0)$ . Performing the limits  $L \rightarrow \infty$  and  $N_T \rightarrow \infty$  with  $N_R = \text{const}$ , we obtain

$$P_{\text{fix}} = 1 - \exp\left(-sN_R \int dx dy f(x, y, 0)\right), \quad (31)$$

which is the generalization, in two dimensions, of the result proved in Ref. [13] for the one-dimensional case.

In the strong noise limit, taking as a reference Eq. (29), the space average population  $f(m)$  behaves as in the case of a well-mixed population of size  $N_T$  growing (or decaying) with a characteristic timescale  $1/N_R D$  and a selective advantage  $s$ . Then the average fixation time should be of the order  $N_T/N_R D \sim L^2/D$ , which is the expected timescale for fixation at  $\vec{v} = 0$ , in the continuous limit of Eq. (11). In contrast, in the weak noise limit the average fixation timescale is of order  $N_T$  and it is independent of the diffusivity  $D$ . In summary, for  $\vec{v} = 0$  our theoretical approach nicely agrees with both theoretical and numerical findings in both one and two dimensions and supports our estimate given in Eq. (27), i.e.,  $t_* = a^2/D$ .

We now turn our attention to the case  $\vec{v} \neq 0$ . In this case the estimate of  $t_*$ , referred to as  $t_u$  in the following, can be done in terms of the effective or eddy diffusivity  $D_{\text{eff}}$  and its corresponding space scale  $l_u$ :

$$t_*(\vec{v} \neq 0) \equiv t_u \sim \frac{l_u^2}{D_{\text{eff}}}. \quad (32)$$

It is possible to show that  $t_u < t_D$ . This inequality can be understood as follows. Let us define  $\tilde{D}_{\text{eff}}$  as the effective diffusivity acting at the deme scale  $a$  over the time  $t_u$ , i.e.,  $\tilde{D}_{\text{eff}} t_u = a^2$ . It follows that  $\tilde{D}_{\text{eff}} = D_{\text{eff}} a^2 / l_u^2$  and we expect the advection to be relevant in the dynamics provided  $\tilde{D}_{\text{eff}} \geq D$ .

Then

$$\tilde{D}_{\text{eff}} = D_{\text{eff}} \frac{a^2}{l_u^2} \geq D \rightarrow t_D \equiv \frac{a^2}{D} \geq \frac{l_u^2}{D_{\text{eff}}} \equiv t_u. \quad (33)$$

The inequality  $t_u < t_D$  implies that the strong noise limit for  $\vec{v} \neq 0$  may be observed only if, for  $\vec{v} = 0$ , the system is in the strong noise regime.

In the presence of an advection velocity field, Eq. (24) now becomes

$$\begin{aligned} \frac{\partial f(m)}{\partial t} = & \frac{\mu}{1 + \frac{\mu l_u^2}{N_0 D_{\text{eff}}}} s f(m) [1 - f(m)] \\ & + \left[ \frac{2}{N_T} \frac{\mu}{1 + \frac{\mu l_u^2}{N_0 D_{\text{eff}}}} f(m) [1 - f(m)] \right]^{1/2}. \end{aligned} \quad (34)$$

As already noted, to understand whether or not the strong noise limit is achieved, the relevant quantity is

$$G_u \equiv \frac{\mu l_u^2}{N_0 D_{\text{eff}}}. \quad (35)$$

For  $G_u \gg 1$ , the system should be considered in the strong noise limit and Eq. (34) becomes

$$\begin{aligned} \frac{\partial f(m)}{\partial t} = & \frac{N_0 D_{\text{eff}}}{l_u^2} s f(m) [1 - f(m)] \\ & + \left[ \frac{2}{N_T} \frac{N_0 D_{\text{eff}}}{l_u^2} f(m) [1 - f(m)] \right]^{1/2}. \end{aligned} \quad (36)$$

There is no simple analytical way to estimate  $D_{\text{eff}}$  and  $l_u$  for a prescribed velocity field  $\vec{v}$ . In some cases, such as the one considered in this paper, an explicit computation of  $D_{\text{eff}}$  and  $l_u$  can be done (see [9,10] for further details). In general, one can introduce a characteristic velocity field  $u_0$  such that  $D_{\text{eff}} = u_0 l_u$ . This is, for instance, the case for a turbulent flow where  $u_0$  is the characteristic scale of the turbulent kinetic fluctuations, on scale  $l_u$ , and  $D_{\text{eff}}$  is obtained by the Richardson diffusion [16]. Using  $D_{\text{eff}} = u_0 l_u$ , the condition  $G_u \gg 1$  becomes  $\mu l_u / N_0 u_0 \gg 1$ , which is the same condition given by Eq. (10) in the Introduction.

Finally, using Eq. (36) and the inequality  $t_u < t_D$ , we obtain, for the average fixation time,

$$\frac{N_T l_u^2}{N_0 D_{\text{eff}}} = \frac{N_T}{N_0} t_u \leq \frac{N_T}{N_0} t_D = \frac{L^2}{D}. \quad (37)$$

The effect of the velocity advection, for large  $G_u$ , is to speed up the characteristic time for the system to reach fixation. This is also another way to understand the inequality  $t_u < t_D$ .

In the next two sections we provide numerical evidence which supports our theoretical discussion and the above conclusions.

### III. NUMERICAL APPROACH

For our numerical investigation, we consider a two-dimensional domain of size  $L = 2\pi$  with a deme size  $a = L/128$ . The numerical method used in the following is based

on the one introduced in Ref. [12] and shortly revised in the Appendix. The velocity field  $\vec{v}$  is given by

$$v_x = u_0 \sin \left[ k \left( y - \frac{L}{2} \right) + \phi(t) \right] \cos \left[ k \left( x - \frac{L}{2} \right) + \phi(t) \right], \quad (38)$$

$$v_y = -u_0 \sin \left[ k \left( x - \frac{L}{2} \right) + \phi(t) \right] \cos \left[ k \left( y - \frac{L}{2} \right) + \phi(t) \right], \quad (39)$$

$$\phi(t) = \delta \sin(\omega t). \quad (40)$$

Using the above choice of  $\vec{v}$ , we can consider three different cases: (i) no flow,  $u_0 = 0$ ; (ii) nonchaotic flow,  $u_0 > 0$  and  $\delta = 0$ ; and (iii) chaotic flow,  $u_0 > 0$  and  $\delta = \delta_0$ . The no-flow case refers to the ‘‘standard’’ FKPP equations already investigated in many papers (see, for instance, [4,5]). The second case corresponds to a nonchaotic cellular flow [17], while the third one corresponds, for a proper choice of  $\delta_0$ , to a chaotic cellular flow. For all cases we set  $k = 8$  and for the chaotic flow case we choose  $\delta_0 = 2$  and  $\omega = 2$ , which ensure the condition for chaotic flow to occur. Finally, throughout our numerical investigation, we consider  $f(x, y, 0) = 0.0625$  to be uniformly distributed in the domain. We study the dynamics of the system as a function of  $N_0$ ,  $u_0$ , and  $D$ .

For cellular flow we can employ the analytical approach developed in Refs. [9,10] to compute  $D_{\text{eff}}$  as a function of  $l_u \equiv 2\pi/k$  and  $u_0$ . We find that for the nonchaotic flow,  $D_{\text{eff}} \sim \sqrt{D u_0} l_u$ , whereas for the chaotic flow,  $D_{\text{eff}} \sim u_0 l_u$ .

Based on the theoretical analysis done in the preceding section, we are interested in computing the quantity  $A$  defined in Eq. (22) and, in particular, we are interested in studying the quantity  $G \equiv A^{-1} - 1$  for the three different cases. Next, using Eq. (27) for  $\vec{v} = 0$  and (32) for  $\vec{v} \neq 0$ , we obtain  $G_{\text{no flow}} \sim \frac{\mu a^2}{N_0 D}$ ,  $G_{\text{nonchaotic flow}} \sim \frac{\mu l_u^2}{N_0 \sqrt{D} l_u u_0}$ , and  $G_{\text{chaotic flow}} \sim \frac{\mu l_u^2}{N_0 u_0 l_u}$ . By relying on these expressions of  $G$  for the cases of no flow, nonchaotic flow, and chaotic flow, we predict three different scaling properties to be observed, namely, (i) different scaling laws as a function of  $D$ , i.e.,  $G_{\text{no flow}} \sim D^{-1}$ ,  $G_{\text{nonchaotic flow}} \sim D^{-1/2}$ , and  $G_{\text{chaotic flow}}$  independent of  $D$ ; (ii) the same scaling properties for all cases as a function of  $N_0$ , i.e.,  $N_0^{-1}$ ; and (iii) diversity in the scaling behavior of  $G_{\text{nonchaotic flow}}$  and  $G_{\text{chaotic flow}}$  as a function of  $u_0$ :  $G_{\text{nonchaotic flow}} \sim u_0^{-1/2}$  and  $G_{\text{chaotic flow}} \sim u_0^{-1}$ .

In addition to the scaling predictions listed above, our theoretical analysis shows that the fixation probability  $P_{\text{fix}}$  [Eq. (2)] depends neither on  $D$  nor on  $u_0$  and it is given by the Kimura formula or by the Doering relation in the limit  $L \rightarrow \infty$ , as already shown for  $u_0 = 0$  in Ref. [5]. In Fig. 1 we support our conclusion by showing  $P_{\text{fix}}$  for  $u_0 = 1$  in the chaotic flow case with  $D = 10^{-3}$  and  $N_0 = 2$ . The black line in the figure represents the trend of the Kimura formula, which agrees extremely well with the numerical results, sketched by purple closed circles.

Next we discuss how we can numerically compute  $A$ . Equation (22) has been derived assuming an average of different realizations. Let us define  $\langle H \rangle_\alpha$  as the value of  $\langle H \rangle$  for the  $\alpha$  realization and  $f(m)_\alpha$  as the corresponding value of  $f(m)$

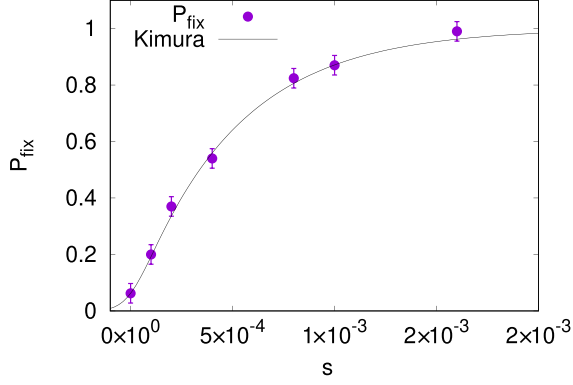


FIG. 1. Fixation probability (purple circles) as a function of the selective advantage  $s$  obtained from a chaotic flow. Simulations were performed with  $N_0 = 2$ , diffusion coefficient  $D = 10^{-3}$ , and  $u_0 = 1$ . The black solid line corresponds to the Kimura formula (2). The error bar is calculated as  $\sqrt{P_{\text{fix}}(1 - P_{\text{fix}})/m}$ , where  $m$  is the number of simulations. For the results shown in the figure,  $m = 500$ .

for the same realization. Both  $\langle H \rangle_\alpha$  and  $f(m)_\alpha$  are functions of time. Then Eq. (22) states that

$$\langle \bar{H} \rangle = A H(\bar{f}(m)), \quad (41)$$

where the overbar is the average over different realizations, i.e.,  $M^{-1} \sum_\alpha \dots$ , with  $M$  the number of realizations. In Fig. 2 we show the quality of the results we obtain for cases of no flow and chaotic flow with  $D = 10^{-3}$  and  $N_0 = 2$ , imposing for the latter case  $u_0 = 1$ :  $\langle \bar{H} \rangle$  is plotted for  $u_0 = 1$  [Fig. 2(a)] and  $u_0 = 0$  [Fig. 2(c)], while the behavior of  $\langle \bar{H} \rangle$  is plotted as a function of  $\bar{f}(m)$  for  $u_0 = 1$  [Fig. 2(b)] and  $u_0 = 0$  [Fig. 2(d)]. We also compute the quantity  $A_\alpha$  for each realization, i.e., we calculate  $A_\alpha$  as the best fit of the relation  $\langle H \rangle_\alpha = A_\alpha H(f(m)_\alpha)$ . The error bars in Fig. 2 refer to three

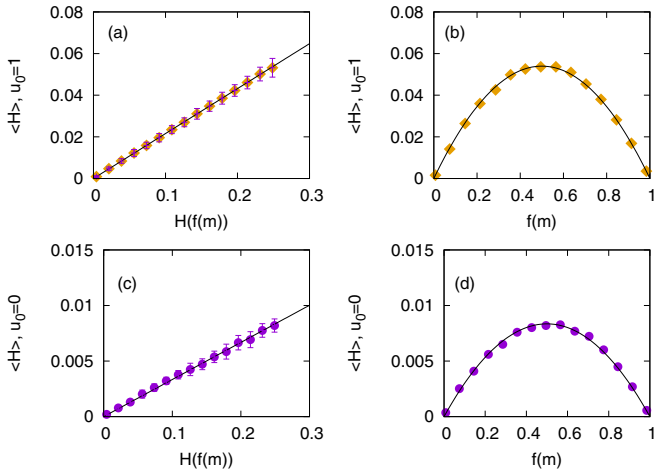


FIG. 2. (a) and (c) Graphs representing the average heterozygosity versus the heterozygosity of the mean value of  $f$  and (b) and (d) plots of the average heterozygosity as a function of the average value of  $f$ . (a) and (b) differ from (c) and (d) because of the presence of the chaotic flow (yellow diamonds). (c) and (d) show the cases with no flow (purple circles). We performed simulations for  $D = 10^{-3}$  and  $N_0 = 2$ . The error bars are 3 times the variance computed over 100 realizations.

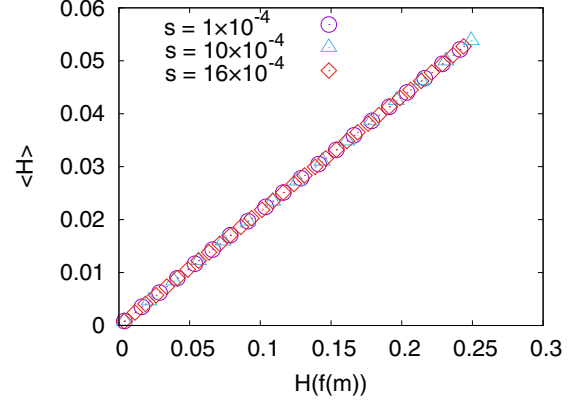


FIG. 3. Average heterozygosity vs heterozygosity of the average value of  $f$  for three different values of the selective advantage  $s$  under a chaotic flow. The parameters are  $N_0 = 2$  and  $D = 10^{-3}$ .

times the variance of  $A_\alpha$ . The same result holds for different values of  $s$  and  $D$ : Overall, from the numerical simulations we can obtain a measure of  $A$  with an accuracy of about 1%.

Next we consider how the computation of  $A$  may eventually depend on  $s$ . In Fig. 3 we show  $\langle \bar{H} \rangle$  as a function of  $H(\bar{f}_m)$  for the chaotic flow case with  $D = 10^{-3}$  and  $s = 10^{-4}$ ,  $10^{-3}$ , and  $1.6 \times 10^{-3}$ ; there is no observable difference in  $A$  for the three different cases. Based on the results of Fig. 3, we can reasonably reach the conclusion that our numerical computation of  $A$  is independent of  $s$ . From the knowledge of  $A$  we can extract the value of  $G = A^{-1} - 1$  for the three different cases of no flow, nonchaotic flow, and chaotic flow.

#### IV. COMPARISON WITH ANALYTICAL ESTIMATE

As stated in the preceding section, we have three different predictions for the scaling  $G = A^{-1} - 1$  for the three cases considered: no flow, nonchaotic flow, and chaotic flow. Prediction (i) refers to the behavior of  $G$  with respect to the diffusivity  $D$ , namely, we expect

$$\begin{aligned} G_{\text{no flow}} &\sim \frac{1}{D}, \\ G_{\text{nonchaotic flow}} &\sim \frac{1}{\sqrt{D}}, \\ G_{\text{chaotic flow}} &\sim \text{const.} \end{aligned} \quad (42)$$

As discussed in Sec. II, the scaling of  $G_{\text{nonchaotic flow}}$  and  $G_{\text{chaotic flow}}$  depends on how the effective or eddy diffusivity  $D_{\text{eff}}$  depends on  $D$ . For both chaotic and nonchaotic flow cases, the effective diffusivity can be computed [10] and we obtain for the nonchaotic case  $D_{\text{eff}} \sim \sqrt{D}$ , whereas for the chaotic case we find  $D_{\text{eff}}$  to be independent of  $D$ . To check the scaling (42) we consider  $D \in [0.0002, 0.016]$  for all cases and we set  $N_0 = 2$ . The results are shown in Fig. 4, where we plot  $G_{\text{no flow}}$ ,  $G_{\text{nonchaotic flow}}$ , and  $G_{\text{chaotic flow}}$  as a function of  $D$ . The two straight lines refer to the scalings  $D^{-1}$  and  $D^{-1/2}$ . For the nonchaotic flow case we show the computation performed at  $u_0 = 1$ , while for chaotic flow case we show two different values of  $u_0$ , namely,  $u_0 = 1$  and  $u_0 = 0.2$ . At a relatively small value of  $D$  the three different scaling behaviors (42) are clearly satisfied. At a relatively large value of  $D$ , the value of

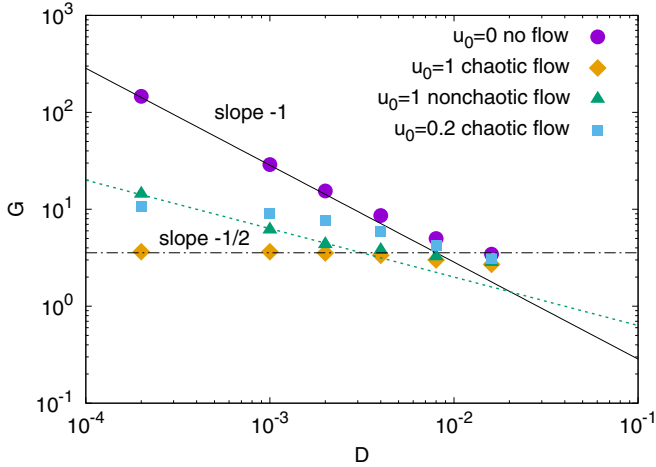


FIG. 4. Values of  $G$  as a function of the diffusion parameter  $D$ . Circles, triangles, squares, and diamonds represent the results of our simulation for different velocity cases: no velocity ( $u_0 = 0$ ), nonchaotic velocity field for the value  $u_0 = 1$ , and chaotic velocity field for the values  $u_0 = 0.2$  and  $1$ , respectively. The solid and dashed lines refer to the linear fit of the simulation results whose slopes are  $-1$  in one case and  $-\frac{1}{2}$  in the other case. The horizontal dot-dashed line shows the constant value achieved for the chaotic flow with  $u_0 = 1$  at very small  $D$ . The error bar is estimated from the error of the best fit; it is smaller than the size of the system, which is why it cannot be seen on the graph.

$G$  decreases and approaches order 1; this should be expected since we know that for  $D$  large enough we enter the so-called weak noise regime and the spatial effects can be neglected. In addition, we can observe that  $G_{\text{nonchaotic flow}}$  and  $G_{\text{chaotic flow}}$  are both smaller compared to  $G_{\text{no flow}}$ , independently of  $D$ . This observation agrees with our theoretical discussion in Sec. II and implies the relation  $t_u < t_D$ .

Next we consider the behavior of  $G$  as a function of  $N_T = N_0 n^2$ . For all cases we should observe that  $G \sim N_T^{-1}$ . To check this prediction, we consider the two cases of no flow and chaotic flow and in Fig. 5 we show  $G_{\text{no flow}}$  and  $G_{\text{chaotic flow}}$  as a function of  $N_0$ . Again, the behavior of  $G$  as

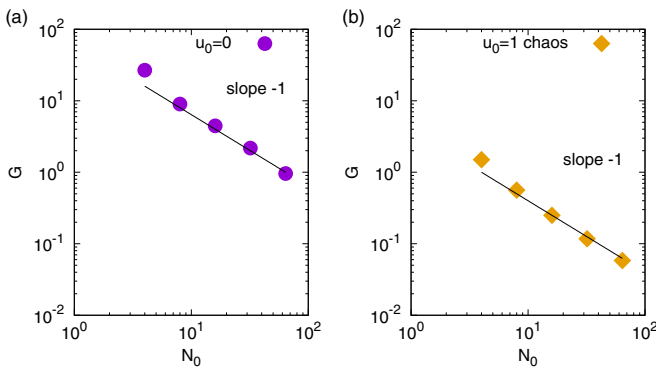


FIG. 5. Values of  $G$  as a function of the number of individuals  $N_0$  per deme for (a) the case of no velocity (purple circles) and (b) the results in the presence of a chaotic flow with  $u_0 = 1$  (yellow diamonds). Both curves follow a slope of  $-1$ . In both cases we use  $D = 10^{-3}$  and  $N_0 \in [4, 64]$ .

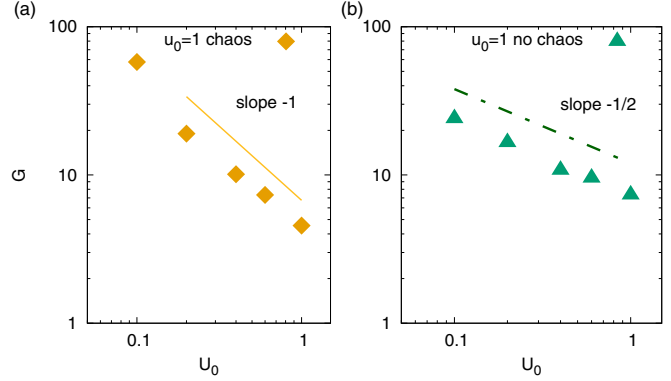


FIG. 6. Values of  $G$  as a function of the velocity intensity  $u_0$  for (a) the results under a chaotic velocity field (yellow diamonds) and (b) the findings in the presence of a nonchaotic velocity field (green triangles). Two different behaviors are shown: (a) The chaotic results follow a slope of  $-1$  whereas (b) the nonchaotic results follow a slope of  $-\frac{1}{2}$ . The numerical parameters used in the simulations are  $N_0 = 2$  and  $D = 10^{-3}$ .

a function of  $N_0$  is rather well satisfied. Combining the results shown in Figs. 4 and 5, we can argue, as already noted in Sec. II, that the continuous limit of Eq. (11) can be achieved by sending  $N_T \rightarrow \infty$  while keeping  $N_T D$  small and constant. In other words, the continuous limit of Eq. (11) is achieved by increasing the domain size at constant density and vanishing diffusivity.

The last prediction discussed in Sec. III applies only to the cases of no flow and chaotic flow and refers to the scaling behavior of  $G$  with respect to the velocity  $u_0$ :

$$G_{\text{nonchaotic flow}} \sim \frac{1}{u_0^{1/2}}, \quad G_{\text{chaotic flow}} \sim \frac{1}{u_0}. \quad (43)$$

In Fig. 6 we show  $G_{\text{nonchaotic flow}}$  and  $G_{\text{chaotic flow}}$  for  $N_0 = 2$ ,  $D = 10^{-3}$ , and  $u_0 \in [0.1, 1]$ . The scaling (43) is verified in both cases.

The results shown in Figs. 4–6 validate the theoretical analysis performed in Sec. II. Without any advection field, the timescale of the dynamics is controlled by the ratio  $G_D = \mu/N_R D$ , where  $N_R = N_T/L^2$  is the population density and the diffusivity plays a relevant role only for  $G_D \gg 1$ . When advection is present, the relevant parameter depends on the effective diffusivity  $D_{\text{eff}}$  and its corresponding length scale  $l_u$  through the combination  $G_u = \mu l_u^2 / N_0 D_{\text{eff}} \leq G_D$ . In general, the functional form of  $D_{\text{eff}}$  depends on the flow properties (as shown in Figs. 4 and 6). For large values of  $G_u$ , the timescale of the dynamics is controlled by the effective diffusivity and by  $l_u$ . In all cases, the fixation probability depends neither on the diffusivity nor on the advection, assumed to be incompressible.

### V. CONCLUSION

In this paper we focused our investigation on the fixation probability between two populations, one of which has a slight selective advantage. In particular, we considered the case of two populations whose dynamics is confined in a closed system and eventually advected by a two-dimensional incom-

pressible flow. We restricted our consideration to the case where initially the two populations are uniformly distributed in space and the one with the selective advantage presents a space density  $f(0) \ll 1$ . For the well-mixed case, when both diffusion and advection are irrelevant, the fixation probability is given by the Kimura theory. For one-dimensional system and without advection, it was shown that the fixation probability does not depend on the value of diffusivity acting in the system [6]. This result was proved by Maruyama [7] and by Pigolotti *et al.* [5] on the basis of numerical simulations arguing that Doering's findings should be true also for the two-dimensional case, yet without advection.

Our paper generalized this previous evidence in several ways. First, we provided a theoretical analysis showing that the fixation probability should be independent of the diffusivity and the effect of the velocity field (if present). We also showed that, without advection, the results in Ref. [6] are recovered for small diffusivity or equivalently for a large system size. Concerning the latter case, we argued theoretically and checked numerically that the dimensionless relevant parameter in the system is the ratio  $\mu/N_R D$ , where  $1/\mu$  is the generation time for the population growth,  $N_R$  is the population density, and  $D$  is the diffusivity. In the strong noise regime, corresponding to  $\mu/N_R D \gg 1$ , the timescale for fixation to occur depends on  $N_R$ ,  $D$ , and  $s$  and we expect fixation to occur on a timescale  $L^2/D$ . Our analysis was generalized to take into account the effect of advection. The relevant dimensionless parameter is now  $\mu l_u^2/N_0 D_{\text{eff}}$ , where  $N_0$  is the number of individuals per deme,  $D_{\text{eff}}$  is the effective or eddy diffusivity induced by the flow, and  $l_u$  is its corresponding length scale. The equivalence of the strong noise regime is given by the condition  $\mu l_u^2/N_0 D_{\text{eff}} \gg 1$ . In this regime, the timescale for fixation is controlled by the flow dynamics. We remarked that the quantity  $\mu l_u^2/N_0 D_{\text{eff}}$  plays the same role as the Damköler number  $\text{Da} = \mu l_u/u_0$  for the continuous equation (with no number fluctuations), where  $u_0$  is the characteristic velocity of the flow field. It is known that, without number fluctuations, the front speed of a population advected by an incompressible velocity field depends on the Damköler and the Péclet number  $u_0 l_u/D$  [10]. When number fluctuations are taken into account, previous theoretical and numerical findings for the continuous case are valid provided  $\mu l_u^2/N_0 D_{\text{eff}} \gg 1$ .

Besides the above results, which nicely generalize many previous findings, one may wonder whether the effect of the advection of an incompressible flow may be relevant for some realistic cases. In particular, we wanted to consider the case of phytoplankton dynamics subject to ocean circulation and turbulence. We assumed that, without advection, the phytoplankton dynamics can be considered to be in the strong noise regime where diffusivity effects control the timescale for a slightly advantageous population to eventually dominate (fixation). This is true, for instance, for a population density of order  $10^7$ – $10^9$  individuals for  $m^3$  with a generation time order of 1 day and size of order  $1 \mu\text{m}$  corresponding to diffusivity order  $10^{-13} \text{ m}^2/\text{s}$ . Depending on the population density, these parameters correspond to  $\mu/N_R D \in [50, 1000]$ . Next we considered the effect of turbulence where we know that the effective diffusivity becomes scale dependent and it can be estimated using the Richardson theory and the Kolmogorov

scaling. Upon defining  $\epsilon$  as the energy dissipation per unit mass of the turbulence flow,  $l$  as the scale where we consider the effect of the effective viscosity  $D_{\text{eff}} \sim \epsilon^{1/3} l^{4/3}$ , and  $N_0 \sim 1$ , the relevant dimensionless quantity becomes  $G_t \equiv \mu l^2/N_0 D_{\text{eff}}$ . An estimate of  $\epsilon$  can be obtained by using the recent analysis performed in Ref. [18], where it was shown that for  $l \sim 10 \text{ km}$  the probability distribution of  $\epsilon$  is close to a log-normal distribution with a most probable value near the surface close to  $\epsilon \sim 10^{-10} \text{ m}^2/\text{s}$ . With these numbers, we obtain  $G_u \sim 10$  and the timescale for fixation to occur becomes order of 10 days. This estimate is clearly very rough since all the variables we considered show strong and even intermittent fluctuations both in space and in time. At any rate, our evaluation of  $G_u$  was just done to illustrate that the advection of a relatively weak compressible flow, for instance, due to a moderate upwelling, may become an important effect on the population dynamics located in the upwelling region, as discussed, e.g., in Ref. [19]. This effect is different for different population sizes, densities, and characteristics of the population (motile versus nonmotile) for different flow characteristics, thus contributing, directly or indirectly, to the well-known complex dynamics of oceanic biomass.

#### ACKNOWLEDGMENT

The authors would like to thank Abigail Plummer for useful discussions.

#### APPENDIX A: NUMERICAL ALGORITHM

In this Appendix we give a brief description of a numerical model to investigate the behavior of population dynamics and genetics under flow, closely following the work of Guccione *et al.* [12]. The model aims to describe the space-time evolution of a population by solving the FKPP equation (11), namely,

$$\frac{\partial f}{\partial t} + \vec{v} \cdot \vec{\nabla} f = D \Delta f + \mu s f(1-f) + \left[ \frac{2\mu}{N_0} f(1-f) \right]^{1/2} w(\vec{x}, t). \quad (\text{A1})$$

The method consists of a series of steps. Let us start by considering a uniform lattice of spacing  $a$ . Every interval  $i = 1, \dots, n$  of size  $a$  spans a region within which there is a number  $N_i^{(\beta)}$  of individuals, where  $\beta = A, B$  refers to the two possible species. In the first step the particles present in the boxes will be displaced due to diffusion and they will be redistributed on a domain  $(1 + \alpha)a^d$ , where  $\alpha$  identifies the diffusion process and  $d$  refers to the dimension of the considered system. We execute a Markov chain with next-neighbor hopping and periodic boundary conditions, whose convergence is related to a diffusion process, with diffusivity constant  $D$ . The hopping probability is defined by

$$p \equiv \frac{D \Delta t}{a^2}, \quad (\text{A2})$$

with  $p \ll 1$ .



*Step 1: Diffusion.* For each interval  $i$ , the position of the particle  $x_\alpha(i)$  is calculated as

$$x_\alpha(i) = (i - \frac{1}{2})a + a(\eta - \frac{1}{2})(1 + 2p), \quad (\text{A3})$$

where  $\eta$  is a uniformly distributed random number within  $[0, 1]$ . If an external velocity field is present then the particles undergo a further displacement in continuous space.

*Step 2: Advection.* The advection is calculated as

$$x_\alpha(i, t + \Delta t) = x_\alpha(i) + u(x_\alpha(i))\Delta t, \quad (\text{A4})$$

where  $u(x, t)$  is a defined advecting field.

We notice that the particles from the box we started from will be moved to another box, thus making a change in the number of individuals present in the new box.

*Step 3: Relabeling.* It is possible to determine the new index as

$$j \equiv \left\lfloor \frac{x_r(i, t + \Delta t)}{\Delta x} \right\rfloor + 1. \quad (\text{A5})$$

*Step 4: Birth and death processes.* Once the previous steps have been completed, it is possible to calculate the birth-death processes according to specific rates,

$$\tilde{N}_j^{(A)} = \tilde{N}_j^{(A)} + 1 \quad \text{at rate } r_b(A), \quad (\text{A6})$$

$$\tilde{N}_j^{(A)} = \tilde{N}_j^{(A)} - 1 \quad \text{at rate } r_d(A), \quad (\text{A7})$$

$$r_b(A) = \mu \Delta t,$$

$$r_d(A) = \mu \Delta t \frac{\tilde{N}_j^{(A)} - 1 + \tilde{N}_j^{(B)}(1 - s)}{N_0},$$

$$\tilde{N}_j^{(B)} = \tilde{N}_j^{(B)} + 1 \quad \text{at rate } r_b(B), \quad (\text{A8})$$

$$\tilde{N}_j^{(B)} = \tilde{N}_j^{(B)} - 1 \quad \text{at rate } r_d(B),$$

$$r_b(B) = \mu \Delta t,$$

$$r_d(B) = \mu \Delta t \frac{\tilde{N}_j^{(B)} - 1 + \tilde{N}_j^{(A)}(1 + s)}{N_0}, \quad (\text{A9})$$

where  $s$  is the selective advantage,  $s > 0$ , or disadvantage,  $s < 0$ , of individuals  $A$  with respect to  $B$ . With  $r_b$  and  $r_d$  the birth and the death probabilities, respectively, are identified.

If the individuals belonging to a given box are known, it is possible to perform this procedure, whose advantage is not tracking the position of each particle. Because of this, in particular, it is possible to consider this method efficient; the computational cost tends to be relatively low.

Note that for each mesh site, the probability to obtain  $k$  new offspring or deaths is binomial and it approximates a Poisson distribution only when the number of individuals considered in the specific process is large enough. This can never happen in proximity to the edge of a propagating front and/or near extinction even for large value of  $N_0$ . Once the last step concludes, we set  $N_j^{(\gamma)} = \tilde{N}_j^{(\gamma)}$  and we can start with a new time step.

In Table I we show the values of the different parameters (except  $s$ ) used in the numerical simulations of the paper. Note that  $N_0 = 2$  is valid for all cases except the one shown in Fig. 5, which in fact displays the value of  $G_u$  as a function of  $N_0$ .

TABLE I. Numerical values used in the simulations.

Parameter	Value
size $L$	$2\pi$
deme size $a$	$\frac{2\pi}{128}$
deme population $N_0$	2
diffusivity $D$	$10^{-3}$

## APPENDIX B: MATHEMATICAL DETAILS FOR INTRODUCING THE CUTOFF $k_M$

In this Appendix we give an explanation regarding the introduction of the cutoff  $k_M$  in the system during the step between Eq. (25) and the relation (26).

By combining Eq. (26) with Eq. (20), i.e.,

$$D \frac{\langle (\vec{\nabla} f)^2 \rangle}{\langle (\delta f)^2 \rangle} = \frac{1}{t_*}, \quad (\text{B1})$$

we get the relation

$$\frac{1}{t_*} = D k_M^2 = \frac{D}{a^2}. \quad (\text{B2})$$

Thus it is possible to derive the timescale  $t_*$  as

$$t_* = \frac{a^2}{D}. \quad (\text{B3})$$

Now, to solve Eq. (25), we calculate a Fourier transform, obtaining

$$\partial_t \phi_k = -k^2 D \phi_k + \sqrt{\epsilon} w_k, \quad (\text{B4})$$

by knowing that the Fourier transform of white noise is a constant. The averages of  $\phi^2$  and  $(\vec{\nabla} \phi)^2$  are, respectively,

$$\langle \phi^2 \rangle = \int k dk \langle \phi_k^2 \rangle, \quad (\text{B5})$$

$$\langle (\vec{\nabla} \phi)^2 \rangle = \int k^2 k dk \langle \phi_k^2 \rangle. \quad (\text{B6})$$

Calculating the average of  $\phi^2$ , we get

$$\langle \phi_k^2 \rangle = \frac{\epsilon}{2k^2 D}, \quad (\text{B7})$$

so that

$$\langle \phi^2 \rangle = \frac{\epsilon}{2D} \int \frac{k dk}{k^2} = \frac{\epsilon}{2D} \ln \left( \frac{k_M}{k_0} \right), \quad (\text{B8})$$

and for the gradient

$$\langle (\vec{\nabla} \phi)^2 \rangle = \frac{\epsilon}{2D} \int \frac{k^2 k dk}{k^2} = \frac{\epsilon}{4D} k_M^2. \quad (\text{B9})$$

Making the relationship between  $\langle \phi^2 \rangle$  and  $\langle (\vec{\nabla} \phi)^2 \rangle$  while keeping apart the natural logarithmic term, we obtain the factor  $k_M$ , which is why it is necessary to introduce the cutoff.

- [1] M. Kimura, On the probability of fixation of mutant genes in a population, *Genetics* **47**, 713 (1962).
- [2] M. Kimura and G. H. Weiss, The stepping stone model of population structure and the decrease of genetic correlation with distance, *Genetics* **49**, 561 (1964).
- [3] M. Kimura and T. Ohta, The average number of generations until fixation of a mutant gene in a finite population, *Genetics* **61**, 763 (1969).
- [4] K. S. Korolev, M. Avlund, O. Hallatschek, and D. R. Nelson, Genetic demixing and evolution in linear stepping stone models, *Rev. Mod. Phys.* **82**, 1691 (2010).
- [5] S. Pigolotti, R. Benzi, P. Perlekar, M. H. Jensen, F. Toschi, and D. R. Nelson, Growth, competition and cooperation in spatial population genetics, *Theor. Popul. Biol.* **84**, 72 (2013).
- [6] C. R. Doering, C. Mueller, and P. Smereka, Interacting particles, the stochastic Fisher-Kolmogorov-Petrovsky-Piscounov equation, and duality, *Physica A* **325**, 243 (2003).
- [7] T. Maruyama, A simple proof that certain quantities are independent of the geographical structure of population, *Theor. Popul. Biol.* **5**, 148 (1974).
- [8] O. Hallatschek and K. S. Korolev, Fisher Waves in the Strong Noise Limit, *Phys. Rev. Lett.* **103**, 108103 (2009).
- [9] L. Biferale, A. Crisanti, M. Vergassola, and A. Vulpiani, Eddy diffusivities in scalar transport, *Phys. Fluids* **7**, 2725 (1995).
- [10] M. Cencini, A. Torcini, D. Vergni, and A. Vulpiani, Thin front propagation in steady and unsteady cellular flows, *Phys. Fluids* **15**, 679 (2003).
- [11] F. Bianco, S. Chibbaro, D. Vergni, and A. Vulpiani, Front speed in reactive compressible stirred media, *Phys. Rev. E* **87**, 042924 (2013).
- [12] G. Guccione, R. Benzi, A. Plummer, and F. Toschi, Discrete Eulerian model for population genetics and dynamics under flow, *Phys. Rev. E* **100**, 062105 (2019).
- [13] C. R. Doering, C. Mueller, and P. Smereka, in *Unsolved Problems of Noise and Fluctuation: UPoN 2002: Third International Conference on Unsolved Problems of Noise and Fluctuations in Physics, Biology, and High Technology*, edited by S. M. Bezrukov, AIP Conf. Proc. No. 665 (AIP, Melville, 2003), pp. 523–530.
- [14] S. Pigolotti and R. Benzi, Selective Advantage of Diffusing Faster, *Phys. Rev. Lett.* **112**, 188102 (2014).
- [15] R. Benzi, M. H. Jensen, D. R. Nelson, P. Perlekar, S. Pigolotti, and F. Toschi, Population dynamics in compressible flows, *Eur. Phys. J.: Spec. Top.* **204**, 57 (2012).
- [16] L. F. Richardson, Atmospheric diffusion shown on a distance-neighbour graph, *Proc. R. Soc. London Ser. A* **110**, 709 (1926).
- [17] M. Abel, A. Celani, D. Vergni, and A. Vulpiani, Front propagation in laminar flows, *Phys. Rev. E* **64**, 046307 (2001).
- [18] B. Pearson and B. Fox-Kemper, Log-Normal Turbulence Dissipation in Global Ocean Models, *Phys. Rev. Lett.* **120**, 094501 (2018).
- [19] A. Plummer, R. Benzi, D. R. Nelson, and F. Toschi, Fixation probabilities in weakly compressible fluid flows, *Proc. Natl. Acad. Sci. USA* **116**, 373 (2019).